Published in final edited form as:
J Bone Miner Res. 2006 October ; 21(10): 1608–1617. doi:10.1359/jbmr.060716.

Quantification of the Roles of Trabecular Microarchitecture and Trabecular Type in Determining the Elastic Modulus of Human Trabecular Bone

Xiaowei S Liu[1], **Paul Sajda**[2], **Punam K Saha**[3], **Felix W Wehrli**[3], and **X Edward Guo**[1]

[1]Bone Bioengineering Laboratory, Department of Biomedical Engineering, Columbia University, New York, New York, USA

[2]Laboratory for Intelligent Imaging and Neural Computing, Department of Biomedical Engineering, Columbia University, New York, New York, USA

[3]Laboratory for Structural NMR Imaging, Department of Radiology, University of Pennsylvania, Philadelphia, Pennsylvania, USA

Abstract

The roles of microarchitecture and types of trabeculae in determining elastic modulus of trabecular bone have been studied in μCT images of 29 trabecular bone samples by comparing their Young's moduli calculated by finite element analysis (FEA) with different trabecular type-specific reconstructions. The results suggest that trabecular plates play an essential role in determining elastic properties of trabecular bone.

Introduction—Osteoporosis is an age-related disease characterized by low bone mass and architectural deterioration. Other than bone volume fraction (BV/TV), microarchitecture of bone is also believed to be important in governing mechanical properties of trabecular bone. We quantitatively examined the role of microarchitecture and relative contribution of trabecular types of individual trabecula in determining the elastic property of trabecular bone.

Materials and Methods—Twenty-nine human cadaveric trabecular bone samples were scanned at 21-μm resolution using a μCT system. Digital topological analysis (DTA) consisting of skeletonization and classification was combined with a trabecular type-specific reconstruction technique to extract the skeleton and identify topological type of trabeculae of the original trabecular bone image. Four different μCT-based finite element (FE) models were constructed for each specimen: (1) original full voxel; (2) skeletal voxel; (3) rod-reconstructed, preserving rod volume and plate skeleton; and (4) plate-reconstructed, preserving plate volume and rod skeleton. For each model, the elastic moduli were calculated under compression along each of three image-coordinate axis directions. Plate and rod tissue fractions directly measured from DTA-based topological classification were correlated with the elastic moduli computed from full voxel model.

Results—The elastic moduli of skeleton models were significantly correlated with those of full voxel models along all three coordinate axes (r^2 = 0.38~0.53). The rod-reconstructed model contained 21.3% of original bone mass and restored 1.5% of elastic moduli, whereas the plate-reconstructed model contained 90.3% of bone mass and restored 53.2% of elastic moduli. Plate tissue fraction showed a significantly positive correlation (r^2 = 0.49) with elastic modulus by a power law, whereas rod tissue fraction showed a significantly negative correlation (r^2 = 0.42).

Address reprint requests to: X Edward Guo, PhD, Department of Biomedical Engineering, Columbia University, 351 Engineering Terrace, Mail Code 8904, 1210 Amsterdam Avenue, New York, NY 10027, USA, ed.guo@columbia.edu.

The authors state that they have no conflicts of interest.

Conclusions—These results quantitatively show that the microarchitecture alone affects elastic moduli of trabecular bone and trabecular plates make a far greater contribution than rods to the bone's elastic behavior.

Keywords

osteoporosis; microarchitecture; trabecular type; digital topology; μCT imaging

INTRODUCTION

Osteoporosis is an age-related disease characterized by low bone mass and architectural deterioration, leading to bone fragility and an increased susceptibility to fractures.[1] Proximal femurs, spines, and distal radii are the most common sites of osteoporotic fractures. In these anatomic locations, trabecular bone predominates and plays critically important role in load transmission and energy absorption.[2–5] Research during the past three decades has shown a strong correlation between BMD and the elastic modulus or strength of trabecular bone. It is believed that fracture risk is significantly determined by BMD reduction.[6] BV/TV and BMD are widely considered as primary predictors of osteoporotic bone fractures. However, even at a given BMD, fracture risk is known to strongly depend on age,[7] leading to a more recently established view that other age-related factors in trabecular bone microstructure need to be identified.

Jensen and Mosekilde[8] modeled the vertebral trabecular bone architecture as a lattice network of thick vertical columns and thinner horizontal struts and showed that the apparent elastic modulus of trabecular bone can vary by as much as a factor of 5–10 from a perfect cubic lattice to a network of maximal irregularity, whereas trabecular bone volume remains almost constant. These findings suggest that the detailed microarchitecture (i.e., the orientation and connection of trabeculae), in addition to bone volume fraction, are also very important in governing the mechanical properties of trabecular bone.

Since the inception of μCT for imaging trabecular bone microstructure,[9] the 2D stereological techniques based on histologic sections have gradually been supplanted by 3D morphological analyses of trabecular bone microstructure.[10–13] The 2D conventional histomorphometric parameters such as trabecular number and separation are estimated given the specific prior assumption of either rod-like or plate-like microstructure.[14] An important parameter characterizing the 3D branched nature of trabecular bone is connectivity.[9,12,15–17] It has been shown that, in the regression between mechanical properties and BV/TV, the inclusion of parameters derived from the above morphological analyses, such as trabecular bone thickness (Tb.Th), trabecular number (Tb.N), trabecular spacing (Tb.Sp), trabecular bone anisotropy, or trabecular connectivity, has improved its predictive power.[16,18–20] However, none of these conventional structural parameters, either individually or in combination, can adequately describe the microarchitecture: how many and what types of trabeculae are in the microstructure and how these trabeculae are connected and oriented, independent of BV/TV.

To study the independent role of trabecular bone microarchitecture, some researchers considered a topological approach to extract the node-and-branch network information from trabecular bone.[21,22] In general, it consists of a skeletonization or thinning process while maintaining the topological features of the trabecular bone network. Results of their experiments indicated that these topological and morphological information can improve predictions of mechanical properties of trabecular bone and be used to monitor trabecular bone loss in patients in conjunction with in vivo μMRI.[23] However, they described the

trabecular bone microarchitecture as a network of interconnected and free lines without considering the morphology and topology of plate-like trabecular microarchitecture.

Wehrli et al.,[24] on the basis of in vivo μMRI structure analysis, first provided in vivo evidence that the trabecular bone loss in osteoporosis patients involves a conversion of trabecular plates to rods and eventual disconnections of trabeculae. This work was based on digital topological analysis (DTA), a method conceived by Saha and colleagues[25–27] and applied to quantitatively characterize trabecular bone networks.[28,29] The trabecular bone skeleton derived by DTA preserves the network's full topological and architectural properties, that is, trabecular types (trabecular plates and rods), trabecular connections, and trabecular orientation. However, the skeletonized microstructure of trabecular bone does not maintain the bone volume information. Therefore, this DTA skeletonization technique offers a unique means to explicitly examine the contributions from trabecular microarchitecture and the distinct trabecular type (plate-like versus rod-like) in determining the elastic modulus of the trabecular bone independent of its bone volume fraction.

In this work, a DTA-based topology-preserving skeletonization and classification technique combined with μCT image–based finite element (FE) modeling was used to quantitatively examine the relationship between the trabecular microarchitecture and elastic modulus of human trabecular bone. Furthermore, rod-like and plate-like trabeculae were separately reconstructed from the skeleton structure with the aid of a newly developed voxel reconstruction technique. The method was applied to quantitatively examine the trabecular types in determining trabecular bone's elastic modulus. In addition, several new morphological parameters were introduced to directly quantify the fraction of different topological types of trabeculae (plate-like versus rod-like) within the original trabecular bone microstructure.

MATERIALS AND METHODS

Trabecular bone sample preparation and μCT imaging

Twenty-nine human trabecular bone samples were obtained from 16 lumbar vertebrae (75.3 ± 13.8 years old, eight males and eight females), 4 proximal femurs (one pair: 60-year-old female; two singles: 64- and 44-year-old males), and one pair of proximal tibias (69-year-old male). The subjects were screened to exclude metabolic bone diseases or bone cancer, and X-ray radiographs were taken to ensure that there was no evidence of damage or other bone pathologies. Twenty 8-mm diameter on-axis (along the principal trabecular orientation) vertebral specimens along the superior-inferior direction were obtained following previously published protocols.[30] Four on-axis specimens from human proximal tibias and five on-axis specimens from proximal femurs were obtained using similar protocols.[31–33] After thawing at room temperature, the cylindrical specimens were aligned and stabilized with wet gauzes in a 15-ml centrifuge tube along their longitudinal axis. The specimen tube was fastened in the specimen holder of a μCT system (vivaCT 40; SCANCO Medical AG, Bassersdorf, Switzerland). The central gauge length of 15 mm was scanned at 21-μm nominal isotropic resolution and the central ~4 × 4 × 4-mm cubical subvolume equivalent to 191 × 191 × 191 voxels was extracted from each reconstructed image. A global thresholding technique was applied to binarize gray-scale μCT images where the minimum between the bone and bone marrow peaks in the voxel gray values histogram was chosen as the threshold value. Isolated voxels or disconnected voxel clusters were removed from binarized μCT images by computing the largest bone component under 26-connectivity.[25,34] The resulting μCT images (Fig. 1A) were used for DTA and FE analyses.

DTA

DTA of a binarized trabecular bone image is accomplished by first performing skeletonization,[27] followed by topological classification.[26] Skeletonization transforms a trabecular bone image into a representation composed of surfaces and curves while preserving the topology (i.e., connectivity, tunnels, and cavities)[25,35] and the rod and plate morphology of the trabecular microarchitecture. Briefly, the skeletonization is an iterative erosion process where bone voxels are peeled off layer by layer until no further bone voxels can be removed without altering the shape or topology of the trabecular microarchitecture. Therefore, the skeleton of a trabecular bone μCT image is essentially a minimal representation of the shape and topology of the trabecular bone microarchitecture (Fig. 1B). After skeletonization of a trabecular bone image, digital topological classification is applied where each skeletal voxel is uniquely classified as a surface or a curve type[26] (Fig. 1C). The method of topological classification is based on the number of objects, tunnels, and cavities in the $3 \times 3 \times 3$ neighborhood of a bone voxel after the latter's hypothetical transformation to a marrow voxel.[26] These topological parameters eventually lead to an unambiguous determination of topological classes (e.g., surface, curve, edge, and junction) at every voxel in the skeletonized representation of a trabecular bone image.

Plate and rod reconstructions

The plate-like and rod-like trabeculae in the original trabecular bone image are referred as "plate" and "rod," respectively, which corresponds to "surface" and "curve" after skeletonization. To examine the relative contribution of plate- and rod-type trabeculae in bone biomechanics, plates and rods were selectively reconstructed from the trabecular bone skeleton. In plate reconstruction, the objective is to fully reconstruct the plate-type trabeculae, which are interconnected by skeletal curves. In other words, in a plate-reconstructed image, plates preserve their thickness or bulk information, whereas rods are represented by skeletal curves (Fig. 1E). On the contrary, in rod reconstruction, the rod-type trabeculae are fully reconstructed from skeletal curves, whereas skeletal surfaces are unaltered. Thus, in a rod-reconstructed image, the rods preserve their thickness information, whereas only skeletal structures are preserved for plates (Fig. 1F).

Plate and rod reconstructions of the trabecular bone image were accomplished by using a topological-type-tagged layer-by-layer reverse filling of bone regions starting from the set of skeletal voxels. In the skeletonization procedure proposed by Saha et al.,[27] bulk bone voxels are iteratively removed in a layer-by-layer fashion, and the iteration number is recorded with each voxel at the time of its removal. During the reverse filling process, all voxels with the same iteration number constitute a layer, and the iteration number represents the depth of the layer. The process starts only with the skeletal voxels as the set of reconstructed voxels, which is subsequently dilated to obtain plate or rod reconstruction of the original trabecular bone. Initially, a topological-type value is assigned to each skeletal voxel by using its DTA-based classification as follows: (1) all surface edge, surface interior, and surface–surface junction voxels are assigned a type value of 1, (2) all curve edge, curve interior, and curve–curve junction voxels are assigned a type value of 2, and (3) all surface–curve junction voxels are assigned a type value of 1.5. In the first reverse filling iteration, the set of reconstructed voxels is dilated to include the voxels in the deepest layer (i.e., the voxels that were deleted in the last iteration during skeletonization). In the next iteration, the dilation process includes the voxels belonging to the next deepest layer, and the process continues until all original bone voxels (the ones that were deleted during skeletonization) are included in the set of reconstructed voxels. During an iteration, the topological type value of a voxel p in the candidate layer is determined as the mean of the topological type values of all previously reconstructed voxels in the $3 \times 3 \times 3$ neighborhood of p. At the end of the reconstruction process, each original bone voxel possesses a type value from the

interval [1, 2], which represents that voxel's topological type index (i.e., likelihood to be a plate-like or rod-like structure). The final type of each reconstructed voxel is determined as follows: if the computed type value is >1.5, it is labeled as a rod-like voxel; if not, it is labeled as a plate-like voxel. Note that surface–curve junctions voxels (type value > 1.5) are eventually labeled as a plate-like voxel. Thus, on completion of the above reconstruction process, each bone voxel in the original bone image is labeled as belonging to either a plate or rod (Fig. 1D). The algorithms of both DTA and reconstructions of plate and rod models were written in Microsoft Visual C^{++} (Microsoft, Redmond, WA, USA) and implemented on a Dell XPS PC workstation (Dell, Round Rock, TX, USA).

FE analyses

Four different μCT images of each specimen, original, skeletonized, rod-reconstructed, and plate-reconstructed images, were converted to a set of voxel-based FE models by converting each voxel to an eight-node brick element. Four μCT-based FE models for each specimen in this study refer to the following: (1) original, full voxel model; (2) skeleton model; (3) rod-reconstructed model; and (4) plate-reconstructed model. The original, full voxel model has the sufficient spatial resolution to appropriately characterize elastic modulus of trabecular bone. The other three models are synthetic models with specific purpose of examining contributions of microarchitecture or trabecular type (rod versus plate). For each model, a linear FE analysis was applied to determine the apparent Young's modulus E* using an element-by-element preconditioned conjugate gradient solver.[36]

The trabecular bone tissue was modeled as an isotropic, linear elastic material with a Young's modulus E_s of 15 GPa and a Poisson's ratio of 0.3.[37] Apparent modulus values were determined along three orthogonal directions: the principal trabecular orientation (*z*) and other transverse directions (*x* and *y*). In each direction, a fixed displacement of $u_i = 0.01$ mm (i = *x*, *y*, and *z*) was applied perpendicularly to one face of the model, whereas the opposite face was imposed zero displacement along the same direction. The total reaction force (RF_i) was calculated from the FE analysis and the apparent Young's modulus E* by the following:

$$E_i^* = \frac{RF_i \ell_i}{u_i A_i},$$

where ℓ_i and A_i were the length and cross-sectional area of the specimen in the *i*th direction (i = *x*, *y*, and *z*), respectively.

Morphological parameters of trabecular bone microstructures

To further describe the microstructure of trabecular bone, the following morphological parameters were also calculated from the labeled bone images: bone volume fraction (BV/TV; the total volume of bone voxels divided by the bulk volume), plate bone volume fraction (pBV/TV; the total volume of plate bone voxels divided by the bulk volume), rod bone volume fraction (rBV/TV; the total volume of rod bone voxels divided by the bulk volume), the plate-to-rod ratio (pBV/rBV; the total volume of plate bone voxels divided by the total volume of rod voxels), plate tissue fraction (pBV/BV; the total volume of plate bone voxels divided by the total volume of bone voxels), rod tissue fraction (rBV/BV; the total volume of rod bone voxels divided by the total volume of bone voxels); and the thinning ratio (the total volume of bone voxels divided by the total volume of skeleton voxels).

Statistical analyses

All the statistical analyses were performed using the Statistic Toolbox in Matlab 6.0 (The MathWorks, Natick, MA, USA) on a PC Workstation. To evaluate the contribution of the microarchitecture to the mechanical properties of trabecular bone, linear correlations between the Young's modulus (E*) of full voxel model and that of the skeleton model were separately studied along all three image coordinate directions. Second, to evaluate the effect of trabecular type on the elastic modulus of entire trabecular bone network, linear correlations between Young's modulus of the full voxel model as well as those of each of the rod- and plate-reconstructed models were separately examined along the three image coordinate axes. The correlation coefficients between BV/TV of full voxel model and those of each of the skeleton and rod-, and plate-reconstructed models were also listed. For the full voxel model, correlations between Young's modulus along principal orientation of trabecular bone specimen (E_z^*) and BV/TV as well as pBV/TV and rBV/TV, which represent the trabecular plate and rod density, were computed. Associations between E_z^* of the full voxel model and trabecular plate tissue fraction (pBV/BV), rod tissue fraction (rBV/BV), and plate-to-rod ratio (pBV/rBV) were evaluated as well. Finally, correlations between thinning ratio and BV/TV as well as E_z^* of the full voxel model were studied.

To differentiate the role of trabecular architecture from bone volume fraction, partial correlation analyses between elastic modulus of full voxel model and those of each of the skeleton and rod-, and plate-reconstructed models along three coordinate axes with the effect of BV/TV removed were performed. Similarly, partial correlation between plate (rod) tissue fraction and E_z^* of the full voxel model with effect of BV/TV removed was studied.

RESULTS

Although the minimal bone volume was maintained in the skeletonized model, surprisingly, there was a significant correlation between E_z^* of the skeleton model and that of full voxel model along the principal orientation of trabecular bone specimens (Fig. 2). Significant correlations were also found in the other two transverse directions (Table 1), with slightly different correlation coefficients. Although the elastic moduli of the skeleton models correlated significantly with those of the original, full voxel models, the values of the skeleton moduli were more than one order of magnitude less than the full moduli values. This, of course, was because the skeletonization led to, on average, a factor of 8.91 reduction in bone volume fraction. Moreover, partial correlation analysis revealed that the correlations between elastic modulus of full voxel model and those of each of the skeleton and rod- and plate-reconstructed models were highly significant even with the effects of BV/TV removed (Table 1).

When trabecular rods were fully reconstructed to their original bone volume in the rod-reconstructed models, the changes in E_z^* from the skeleton model were negligible in terms of the correlation between E_z^* of the rod-reconstructed model and that of full voxel model (Fig. 2). On average, the rod-reconstructed model had a bone tissue volume, which corresponded to 21.3% of the original bone tissue volume. However, the rod-reconstructed model only represented 1.5% of the original elastic modulus. On the other hand, when trabecular plates were fully reconstructed to their original bone volume in the plate-reconstructed models, the changes in elastic modulus from the skeleton model were quite dramatic (Fig. 2). The plate-reconstructed models had 90.3% of the original bone tissue volume and 53.2% of the original elastic modulus on average. The results in the other two transverse directions were similar (Table 1). These observations in elastic modulus are consistent with the results in bone volume fraction, shown in Fig. 3, which suggest that the plate-reconstructed model

maintained most of the bone volume fraction compared with the rod-reconstructed and skeletonized model.

The trabecular bone microstructure in the specimens studied ranges from rod-dominant to plate-dominant, with the plate-to-rod ratios ranging from 4.6 to 29.7. Figure 4 shows the full voxel models and skeleton models of three trabecular bone samples, illustrating the variations in structure type from plate- to rod-dominant. The elastic moduli E_z^* of these samples were also listed and indicated a direct relationship with the plate-to-rod ratio. In Fig. 5A, E_z^* of the full voxel model correlated significantly with the plate bone volume fraction (pBV/TV) by a nonlinear regression of power law, whereas no significant correlation was found between E_z^* and rod bone volume fraction (rBV/TV; Fig. 5B). It should be noted that the pBV/TV combines trabecular type and bone volume fraction. To isolate the effect of the bone volume fraction, pBV/TV and rBV/TV were normalized by BV/TV to obtain plate tissue fraction (pBV/BV) and rod tissue fraction (rBV/BV). Plate or rod tissue fraction represents the percentage of bone tissue belonging to the trabecular plate or rod and the sum of them always equals 1. The correlations between pBV/BV and E_z^*, and between rBV/BV and E_z^* are shown in Figs. 5C and 5D to follow nonlinear regression of power laws. Both correlations were significant ($r^2 = 0.49$ and 0.42, $p < 0.001$) but have opposite signs. Furthermore, partial correlation analysis showed plate (rod) fraction significantly correlated to Young's modulus of the full model ($r^2 = 0.22$, $p = 0.01$) with the effect of BV/TV removed. Finally, correlations between E_z^* and BV/TV and between E_z^* and plate-to-rod ratio are shown in Figs. 5E and 5F.

Assuming the skeleton model represents the medial line or surface of trabeculae, the calculated thinning ratio is a measure of the layers of bone mass build up over the skeleton of the bone. The averaged thinning ratio of studied trabecular bone specimens was 8.9 ± 1.7. No correlation ($r^2 = 0.03$ and 0.005, $p > 0.05$) was found between thinning ratios and either BV/TV or elastic modulus of the full trabecular bone model, suggesting the overall "thickness" of trabecular bone is independent of either BV/TV or elastic modulus.

DISCUSSION

Previous studies have shown relationships between microarchitecture and the elastic modulus or stiffness of trabecular bone in terms of one or several properties of the microarchitecture. This study used a DTA-based skeleton model to represent the full microarchitecture of human trabecular bone as a means to separate the effect of microarchitecture from bone volume fraction. The observation that elastic moduli of skeleton models are significantly correlated with those of full models is intriguing. The partial correlation between the elastic moduli of skeleton models and those of full models further suggests that the skeleton of the trabecular bone, which is the representative of the network's topology, affects its mechanical properties in a manner independent of bone volume fraction. Certainly, bone volume fraction is also a significant factor, which determines elastic modulus of trabecular bone (Fig. 5E). Bone volume fraction is highly correlated with the elastic modulus, which begs the question whether trabecular bone microarchitecture determines the bone volume fraction. Figure 3 shows that, although the skeleton has lost most of the bone volume, BV/TV of skeleton model is still significantly correlated with full BV/TV. Thus, the data suggests that the microarchitecture of trabecular bone may have a direct relationship to BV/TV, which is consistent with previous 2D analyses.[38,39] To examine this question, we introduce a thinning ratio that is a measure of the layers of bone mass build up over the skeleton of the bone. The averaged thinning ratio represents an overall "thickness" of trabecular bone and is independent of either BV/TV or elastic modulus of the full trabecular bone model. Therefore, we can postulate that bone

mass is uniformly rather than randomly built based on the architecture-preserved skeleton. According to this conclusion, bone volume fraction may also be determined by its microarchitecture.[38,39] Our results are consistent with previous studies showing that the deterioration of trabecular architecture resulting from bone remodeling has much greater impact on the elastic modulus and strength of trabecular bone than mere thinning, which does not change microarchitecture of trabecular bone.[40]

A key observation of this study concerns the role of trabecular types in determining the mechanical competence of trabecular bone. The plate-reconstructed model represents a hypothetical trabecular bone structure, which has lost most of the rod-like trabecular volume information while maintaining all plate-like trabeculae and the skeleton of rod-like trabeculae. In contrast, the rod-reconstructed model keeps all rod-like trabeculae while preserving the skeleton of plate-like trabeculae. Our results show that the loss of trabecular rod volume insignificantly affects either elastic modulus or overall bone volume fraction compared with the loss of plate volume (Figs. 2 and 3). Moreover, the elastic modulus is significantly correlated with pBV/TV, whereas no correlation exists between it and rBV/TV (Figs. 5A and 5B). These results support the hypothesis that trabecular plates play a much more important role in determining the elastic modulus and bone volume fraction than do rods. Perforation or disconnection of the trabecular bone elements caused by bone remodeling changes the microarchitecture by reducing the connectivity, and converting trabecular plates to trabecular rods, therefore diminishing elastic modulus of the bone.

In this work, a direct measurement of the trabecular type was introduced. Plate and rod tissue fractions quantitatively indicate the percentage of the bone tissue that belongs to either trabecular type. In this manner, the quantitative influence of trabecular types on elastic modulus of trabecular bone has been shown (Figs. 5C and 5D). An alternative approach toward characterizing trabecular bone type is the structural model index (SMI), which is a measure of the bone's degree of plate-likeness or rod-likeness in the form of an index ranging from 0 to 3.[41] We evaluated the SMI for all 29 samples using the software on the vivaCT 40 (Scanco Medical AG) and compared them with the plate-to-rod ratio. A significant linear correlation existed between the SMI and the plate-to-rod ratio ($r^2 = 0.85$, $p < 0.001$). It should be emphasized that our new trabecular type measures has an advantage of identifying structural elements as belonging to a particular trabecular type rather than a statistical calculation.

The accuracy of μCT-based FE analyses is influenced by the resolution of the image.[42,43] In general, at least three to four voxels across a trabecula are required to adequately model a trabecula. Our skeleton, rod- and plate-reconstructed models are synthetic ones, which only maintain certain aspect of microarchitecture. For example, the skeleton model contains the basic microarchitecture of trabecular bone but it does not represent well the individual trabeculae, because the skeleton model is only one voxel thick. However, the elastic modulus of this synthetic, skeleton model can be used as an indicator of microarchitecture of the full voxel model. It should be noted that in either rod-reconstructed or plate-reconstructed models, the other trabecular type (trabecular plates in the rod-reconstructed model or trabecular rods in the plate-reconstructed model) is artificially one voxel thick. Trabecular type thus can be potentially influenced by the image resolution. However, increasing spatial resolution will not change any major findings in the study. For example, the rod-reconstructed model with a hypothetical 10-μm resolution would have 10-μm-thick trabecular plate skeleton and its elastic modulus would not get any closer to that of the full voxel model. The other limitation of the study is the relatively small sample size of specimens, although the normal distributed BV/TV and elastic modulus do represent a typical trabecular bone population. Finally, the study is completely based on 3D μCT image analysis. Given the discrepancies between 3D μCT analysis and 2D histomorphometric

analysis, more 3D image analysis techniques for μCT such as the one presented in this study should be developed and compared with the traditional 2D analyses.[44,45]

In this study, we evaluated for the first time the full microarchitecture of trabecular bone in terms of the trabecular elements' topology and quantitatively showed these quantities to be independent factors in determining the elastic modulus of trabecular bone. The data also suggest microarchitecture to be an essential determinant of bone volume fraction. Trabecular plate type, as one of the descriptors of microarchitecture, significantly correlates with both BV/TV and elastic modulus. Earlier research qualitatively showed a dramatic change of trabeculae from plate-like to rod-like occurs with aging and osteoporosis, resulting in a decrease of mechanical competence.[46,47] Therefore, the great clinical potential from this study is a new microarchitecture description, with trabecular types that can be used to develop a better understanding of the mechanism of bone loss and corresponding changes in elastic modulus. The function of the microarchitecture and trabecular type is not only an assessment of fracture risk, but also can be used to evaluate the efficacy of pharmaceutical treatment. With the available clinical μCT, the architectural and trabecular type parameters developed in this study could be added to the standard BMD measures as additional indicators for pharmaceutical treatments of osteoporosis. For example, it is important to initiate the treatment for osteoporosis before the dramatic change of microarchitecture and reduction of plate tissue fraction caused by the thinning process of aging or postmenopausal osteoporosis. Although the bone mass of trabecular rods has a minimal contribution to both BV/TV and elastic modulus, the existence of the structure is essential to maintain the integrity of trabecular bone network and its mechanical properties. Various anatomic sites determine the different biomechanical functions of trabecular bone, maintaining a certain percentage of trabecular rods optimize the balance of mechanical competence and the energy to maintain the physiological environment. As the weakest link in the lattice of bone, percentage and properties of trabecular rod may play an important role in the initiation of trabecular bone failure, which is a topic for further study.

Acknowledgments

We thank Dr Tony M Keaveny and Grant Bevill of Berkeley Orthopaedic Biomechanics Laboratory for providing vertebral trabecular bone images. This work was partially supported by grants from National Institutes of Health (AR049613, AR048287, AR041443, AR051376, and AR049553).

References

1. Concensus Development Conference: Prophylaxis and treatment of osteoporosis. Osteoporos Int. 1991; 1:114–117. [PubMed: 1790392]
2. Hansson TH, Roos B, Nachemson A. The bone mineral content and ultimate compressive strength of lumbar vertebrae. Spine. 1980; 5:46–54. [PubMed: 7361198]
3. McBroom RJ, Hayes WC, Edwards WT, Goldberg RP, White AAI. Prediction of vertebral body compressive fracture using quantitative tomography. J Bone Joint Surg Am. 1985; 67:1206–1214. [PubMed: 4055845]
4. Mosekilde L. Normal vertebral body size and compressive strength: Relations to age and to vertebral and iliac trabecular bone compressive strength. Bone. 1986; 7:207–212. [PubMed: 3768199]
5. Silva MJ, Keaveny TM, Hayes WC. Load sharing between the shell and centrum in the lumbar vertebral body. Spine. 1997; 22:140–150. [PubMed: 9122793]
6. Rice JC, Cowin SC, Bowman JA. On the dependence of the elasticity and strength of cancellous bone on apparent density. J Biomech. 1988; 21:155–168. [PubMed: 3350829]
7. Hui SL, Slemenda CW, Johnston CCJ. Age and bone mass as predictors of fracture in a prospective study. J Clin Invest. 1988; 81:1804–1809. [PubMed: 3384952]

8. Jensen KS, Mosekilde L. A model of vertebral trabecular bone architecture and its mechanical properties. Bone. 1990; 11:417–423. [PubMed: 2078435]
9. Feldkamp LA, Goldstein SA, Parfitt AM, Jesion G, Kleerekoper M. The direct examination of three-dimensional bone architecture in vitro by computed tomography. J Bone Miner Res. 1989; 4:3–11. [PubMed: 2718776]
10. Parfitt AM. Age-related structural changes in trabecular and cortical bone: Cellular mechanisms and biomechanical consequences. Calcif Tissue Int. 1984; 36(Suppl 1):S123–S128. [PubMed: 6430512]
11. Whiterhouse WJ. The quantitative morphology of anisotropic trabecular bone. J Microsc. 1974; 101:153–168. [PubMed: 4610138]
12. Odgaard A. Three-dimensional methods for quantification of cancellous bone architecture. Bone. 1997; 20:315–328. [PubMed: 9108351]
13. Odgaard A, Jensen EB, Gundersen HJ. Estimation of structural anisotropy based on volume orientation. J Microsc. 1990; 157:149–162. [PubMed: 2313683]
14. Parfitt AM, Mathews CH, Villanueva AR, Kleerekoper M, Frame B, Rao DS. Relationships between surface, volume, and thickness of iliac trabecular bone in aging and in osteoporosis. Implications for the microanatomic and cellular mechanisms of bone loss. J Clin Invest. 1983; 72:1396–1409. [PubMed: 6630513]
15. Compston JE. Connectivity of cancellous bone: Assessment and mechanical implications. Bone. 1994; 15:463–466. [PubMed: 7980955]
16. Kabel J, Odgaard A, van Rietbergen B, Huiskes R. Connectivity and the elastic properties of cancellous bone. Bone. 1999; 24:115–120. [PubMed: 9951779]
17. Kinney JH, Ladd AJ. The relationship between three-dimensional connectivity and the elastic properties of trabecular bone. J Bone Miner Res. 1998; 13:839–845. [PubMed: 9610748]
18. Goulet RW, Goldstein SA, Ciarelli MJ, Kuhn JL, Brown MB, Feldkamp LA. The relationship between the structural and orthogonal compressive properties of trabecular bone. J Biomech. 1994; 27:375–389. [PubMed: 8188719]
19. Van Rietbergen B, Odgaard A, Kabel J, Huiskes R. Relationships between bone morphology and bone elastic properties can be accurately quantified using high-resolution computer reconstructions. J Orthop Res. 1998; 16:23–28. [PubMed: 9565069]
20. Zysset PK, Sonny M, Hayes WC. Morphology-mechanical property relations in trabecular bone of the osteoarthritic proximal tibia. J Arthroplasty. 1994; 9:203–216. [PubMed: 8014652]
21. Pothuaud L, Porion P, Lespessailles E, Benhamou CL, Levitz P. A new method for three-dimensional skeleton graph analysis of porous media: Application to trabecular bone architecture. J Microsc. 2000; 199:149–161. [PubMed: 10947908]
22. Pothuaud L, Van Rietbergen B, Mosekilde L, Beuf O, Levitz P, Benhamou CL, Majumdar S. Combination of topological parameters and bone volume fraction better predicts the mechanical properties of trabecular bone. J Biomech. 2002; 35:1091–1099. [PubMed: 12126668]
23. Pothuaud L, Newitt DC, Lu Y, MacDonald B, Majumdar S. *In vivo* application of 3D-line skeleton graph analysis (LSGA) technique with high-resolution magnetic resonance imaging of trabecular bone structure. Osteoporos Int. 2004; 15:411–419. [PubMed: 15022037]
24. Wehrli FW, Gomberg BR, Saha PK, Song HK, Hwang SN, Snyder PJ. Digital topological analysis of *in vivo* magnetic resonance microimages of trabecular bone reveals structural implications of osteoporosis. J Bone Miner Res. 2001; 16:1520–1531. [PubMed: 11499875]
25. Saha PK, Chaudhuri BB. Detection of 3-D simple points for topology preserving. IEEE Trans Pattern Anal Mach Intell. 1994; 16:1028–1032.
26. Saha PK, Chaudhuri BB. 3D Digital Topology under Binary Transformation with Applications. Comput Vis Image Underst. 1996; 63:418–429.
27. Saha PK, Chaudhuri BB, Majumder DD. A new shape preserving parallel thinning algorithm for 3D digital images. Pattern Recog. 1997; 30:1939–1955.
28. Saha PK, Gomberg BR, Wehrli FW. Three-dimensional digital topological characterization of cancellous bone architecture. Int J Imaging Syst Technol. 2000; 11:81–90.
29. Gomberg BR, Saha PK, Song HK, Hwang SN, Wehrli FW. Topological analysis of trabecular bone MR images. IEEE Trans Med Imaging. 2000; 19:166–174. [PubMed: 10875701]

30. Kopperdahl DL, Keaveny TM. Yield strain behavior of trabecular bone. J Biomech. 1998; 31:601–608. [PubMed: 9796682]
31. Chang WC, Christensen TM, Pinilla TP, Keaveny TM. Uniaxial yield strains for bovine trabecular bone are isotropic and asymmetric. J Orthop Res. 1999; 17:582–585. [PubMed: 10459766]
32. Morgan EF, Keaveny TM. Dependence of yield strain of human trabecular bone on anatomic site. J Biomech. 2001; 34:569–577. [PubMed: 11311697]
33. Keaveny TM, Guo XE, Wachtel EF, McMahon TA, Hayes WC. Trabecular bone exhibits fully linear elastic behavior and yields at low strains. J Biomech. 1994; 27:1127–1136. [PubMed: 7929462]
34. Hoshen J, Kopelman R. Percolation and cluster distribution. I. Cluster multiple labeling technique and critical concentration algorithm. Phys Rev B. 1976; 14:3438–3445.
35. Saha PK, Chaudhuri BB, Chanda B, Dutta Majumder D. Topology Preservation in 3D digital space. Pattern Recog. 1994; 27:295–300.
36. Hollister SJ, Brennan JM, Kikuchi N. A homogenization sampling procedure for calculating trabecular bone effective stiffness and tissue level stress. J Biomech. 1994; 27:433–444. [PubMed: 8188724]
37. Guo XE, Goldstein SA. Is trabecular bone tissue different from cortical bone tissue? Forma. 1997; 12:185–196.
38. Chappard D, Legrand E, Haettich B, Chales G, Auvinet B, Eschard JP, Hamelin JP, Basle MF, Audran M. Fractal dimension of trabecular bone: Comparison of three histomorphometric computed techniques for measuring the architectural two-dimensional complexity. J Pathol. 2001; 195:515–521. [PubMed: 11745685]
39. Thomsen JS, Ebbesen EN, Mosekilde L. Relationships between static histomorphometry and bone strength measurements in human iliac crest bone biopsies. Bone. 1998; 22:153–163. [PubMed: 9477239]
40. Guo XE, Kim CH. Mechanical consequence of trabecular bone loss and its treatment: A three-dimensional model simulation. Bone. 2002; 30:404–411. [PubMed: 11856649]
41. Hildebrand T, Ruegsegger P. A new method for the model independent assessment of thickness in three-dimensional images. J Microsc. 1997; 185:67–75.
42. Guldberg RE, Hollister SJ, Charras GT. The accuracy of digital image-based finite element models. J Biomech Eng. 1998; 120:289–295. [PubMed: 10412392]
43. Niebur GL, Yuen JC, Hsia AC, Keaveny TM. Convergence behavior of high-resolution finite element models of trabecular bone. J Biomech Eng. 1999; 121:629–635. [PubMed: 10633264]
44. Chappard D, Retailleau-Gaborit N, Legrand E, Basle MF, Audran M. Comparison insight bone measurements by histomorphometry and microCT. J Bone Miner Res. 2005; 20:1177–1184. [PubMed: 15940370]
45. Hordon LD, Itoda M, Shore PA, Shore RC, Heald M, Brown M, Kanis JA, Rodan GA, Aaron JE. Preservation of thoracic spine microarchitecture by alendronate: Comparison of histology and microCT. Bone. 2006; 38:444–449. [PubMed: 16361121]
46. Ding M, Hvid I. Quantification of age-related changes in the structure model type and trabecular thickness of human tibial cancellous bone. Bone. 2000; 26:291–295. [PubMed: 10710004]
47. Laib A, Kumer JL, Majumdar S, Lane NE. The temporal changes of trabecular architecture in ovariectomized rats assessed by MicroCT. Osteoporos Int. 2001; 12:936–941. [PubMed: 11804020]

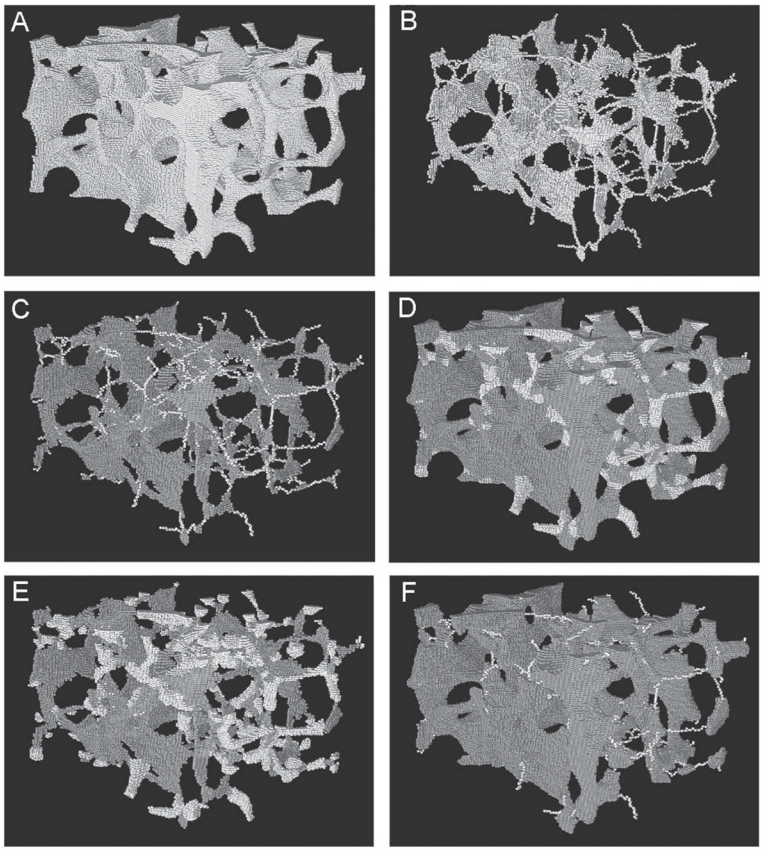

FIG. 1.

Results of DTA and reconstruction procedure on image of vertebral trabecular bone sample ($3.2 \times 3.2 \times 2.1$ mm^3). (A) An original μCT image (full voxel model) of a trabecular bone sample. (B) Skeletonized image (skeleton model) of A. (C) Results of topological classification of B. Plate voxels are shown as dark gray, rod voxels in lighter shading. (D) Reconstructed structures with the trabecular type labeled for each voxel. (E) Rod-reconstructed model. (F) Plate-reconstructed model.

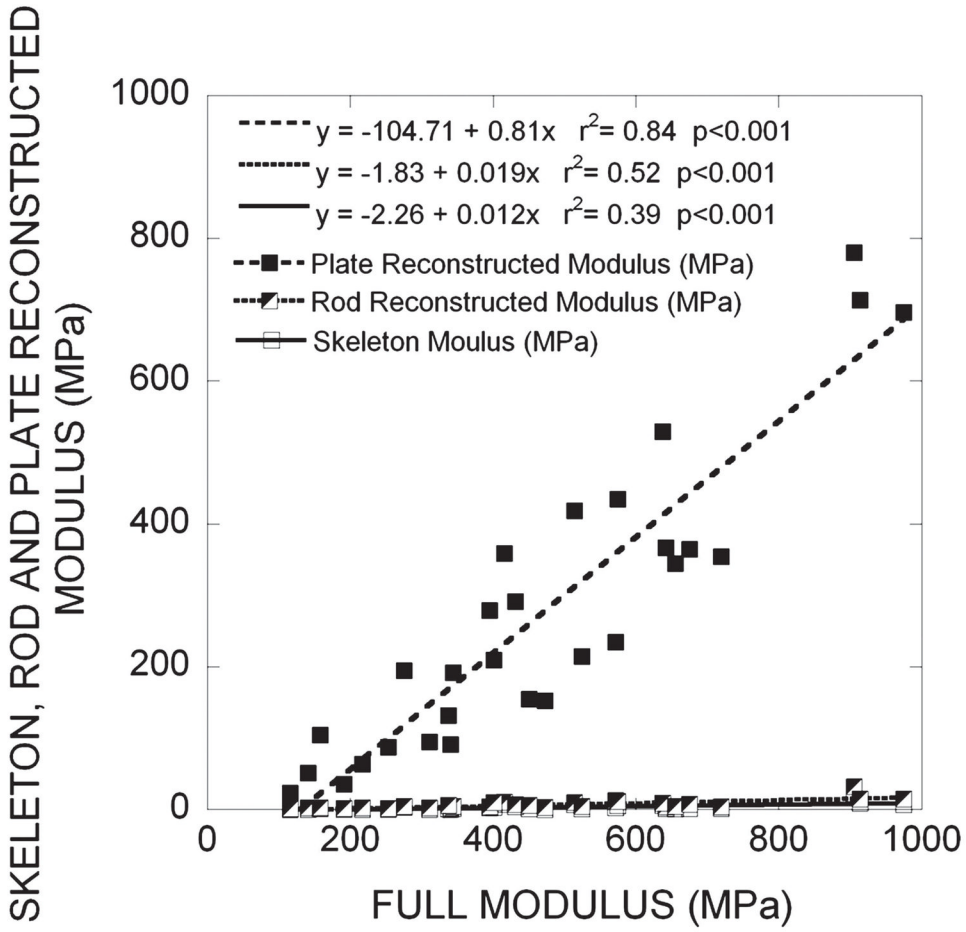

FIG. 2.

Results of linear correlation analyses between the elastic modulus of the full voxel model and that of each of skeleton and plate- and rod-reconstructed models. The plots for the skeleton and rod-reconstructed models were almost superimposed on each other. For the results shown here, the elastic moduli were computed under compression along the *z*-axis of the image which was aligned with the principal orientation of trabeculae.

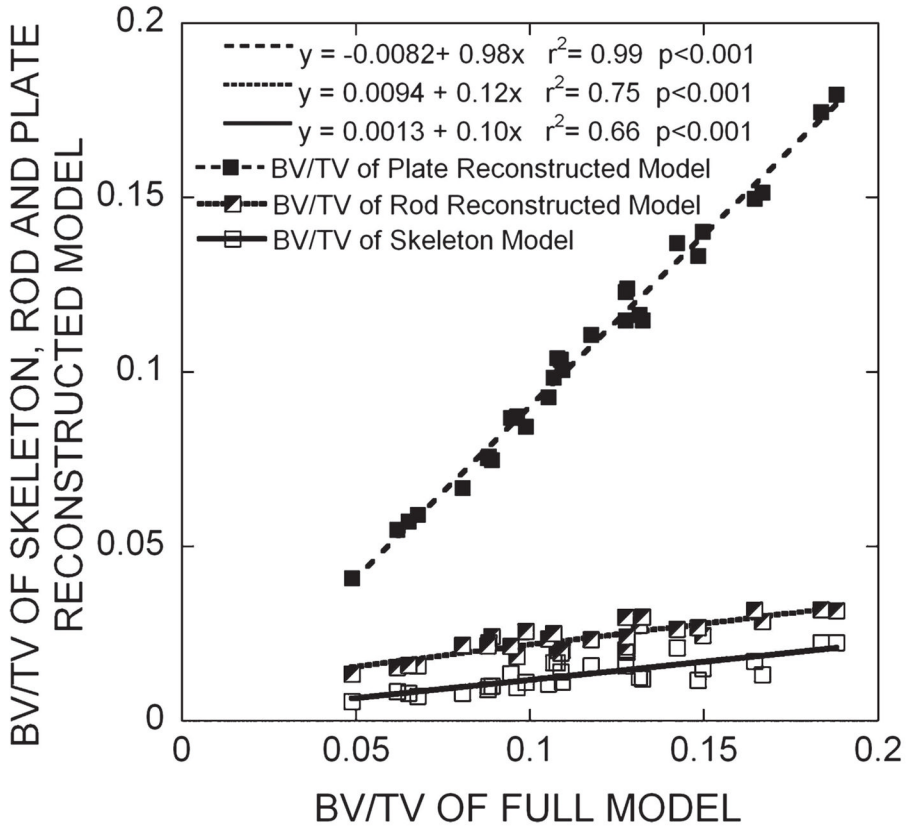

FIG. 3.
Results of linear correlation analyses between the BV/TV of the full voxel models and that of each of skeleton and plate-and rod-reconstructed models.

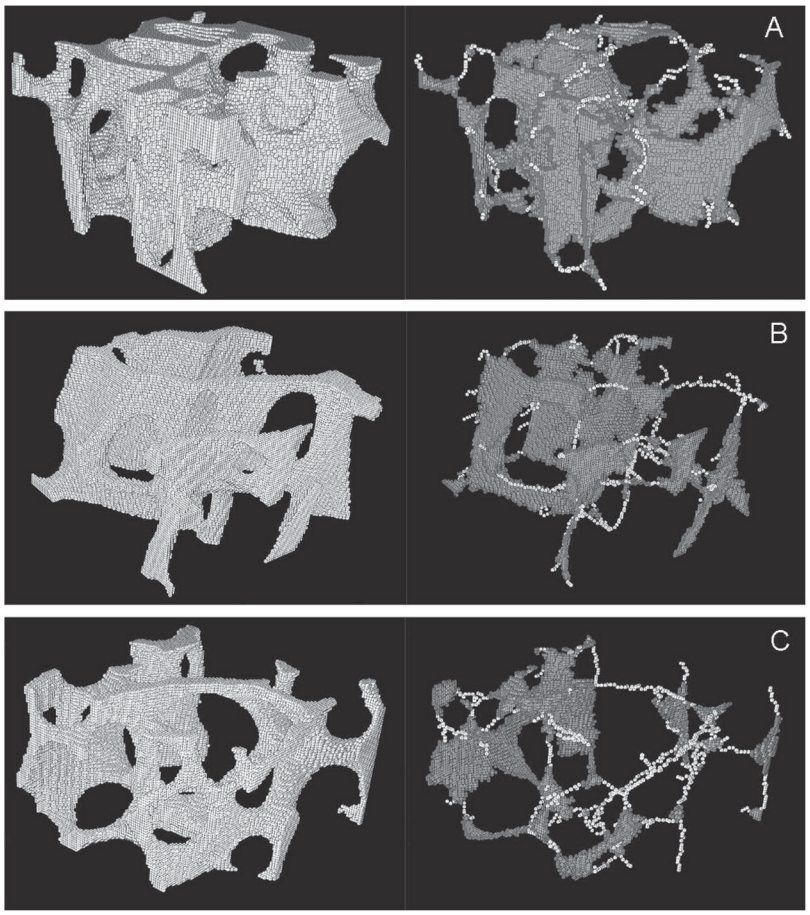

FIG. 4.

Illustrations of DTA on μCT images of three different trabecular bone samples (2.1 × 2.1 × 1.3 mm^3). (Left) Original μCT image (full voxel model) of the trabecular bone sample. (Right) Skeletonized image (skeleton model). (A) Plate-to-rod ratio = 20.10, plate tissue fraction = 0.9526, Young's modulus = 974.8 MPa. (B) Plate-to-rod ratio = 10.22, plate tissue fraction = 0.9109, Young's modulus = 674.8 MPa. (C) Plate-to-rod ratio = 5.94, plate tissue fraction = 0.8559, Young's modulus = 216.8 MPa.

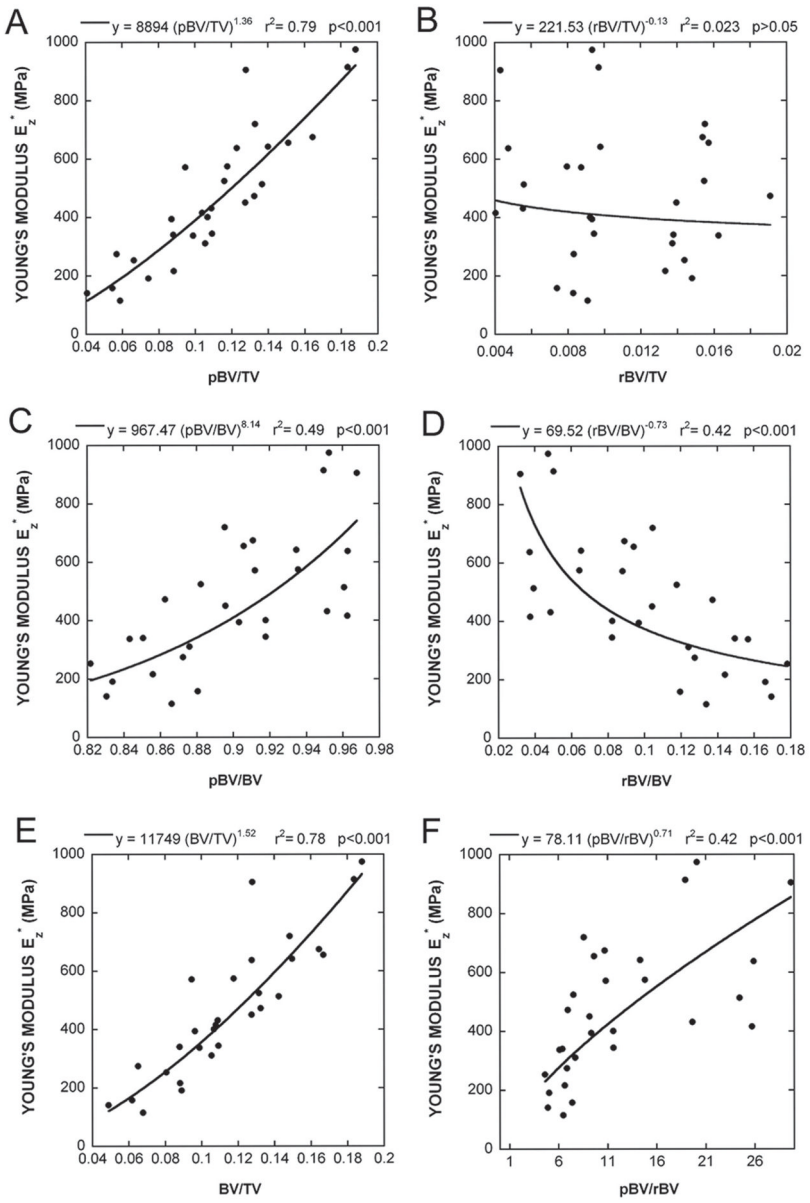

FIG. 5.

Results of correlation analyses between Young's modulus E_z^* of the full voxel model and that of (A) plate bone volume fraction (pBV/TV), (B) rod bone volume fraction (rBV/TV), (C) plate tissue fraction (pBV/BV), (D) rod tissue fraction (rBV/BV), (E) bone volume fraction (BV/TV), and (F) plate-to-rod ratio (pBV/rBV) by nonlinear regression of power laws.

Table 1

Correlation Coefficients* Between Young's Modulus of Trabecular Bone Computed From the Full Voxel Model and That Computed From Each of the Plate- and Rod-Reconstructed and Skeleton Models

	z-axis	y-axis	x-axis
E* (plate)	0.84 (0.70)†	0.84 (0.66)†	0.83 (0.76)†
E* (rod)	0.52 (0.68)†	0.48 (0.34)†	0.67 (0.68)†
E* (skeleton)	0.39 (0.57)†	0.38 (0.34)†	0.53 (0.58)†

Young's moduli were separately computed under compressions along each of three image coordinate axes directions.

*$p < 0.005$ for all correlations in Table 1.

†Partial correlation with the effect of BV/TV removed.